The effects of thermal gradients on the Mars Observer Camera primary mirror

Roger W. Applewhite

Altadena Instruments Corporation
Post Office Box 60077, Catalina Station, Pasadena, California 91116

Arthur R. Telkamp

OCA Applied Optics
7421 Orangewood Avenue, Garden Grove, California 92641

ABSTRACT

The main imaging system of the Mars Observer Camera (MOC) is a Cassegrain telescope which will return high resolution images of the surface of Mars as part of the Mars Observer mission to be launched in September 1992. The primary mirror of the telescope is 13.84 inches in diameter and fabricated from fused silica. To make it stiff but lightweight, the mirror was designed with a "single arch" rear surface contour. After mirror design and fabrication was complete, it was determined through thermal simulation of mission conditions that the primary mirror would experience large radial temperature gradients (as well as small axial and circumferential gradients) during imaging. It was originally thought these gradients would produce uncontrollable aberrations. However, it was determined through finite element analysis that the radius of curvature (ROC) of the reflective surface of this thin mirror changes in a nearly linear fashion with the radial temperature gradient. In addition, a radial gradient only produces a ROC change, without any significant additional surface figure deformation that might cause image degradation. This effect was subsequently utilized in a primary mirror thermal control system which will allow ground control of the ROC, and hence, the focus of the MOC. The effect of radial gradient and the thermal control system were interferometrically tested in a thermal-vacuum chamber (to simulate mission conditions) and the results confirmed the analysis and the viability of the thermal control approach.

1. INTRODUCTION

The Mars Observer Camera (MOC), to be launched on the Mars Observer spacecraft in September of 1992, is a Cassegrain telescope (3.5-meter focal length, f/10). It utilizes the spacecraft's motion to scan a line-array CCD across the Martian surface to create photographic swaths at 1.4-meter per pixel resolution from an altitude of 390 km. The depth of focus of this instrument is very small, 0.00465 inches, which makes it extremely sensitive to variations in the optical geometries utilized. Specifically, the surface figure of the primary mirror and the metered distance between the primary mirror and secondary mirror have a large effect on the performance of the camera. As these components are susceptible to thermal displacement, a unique constraint is placed on the thermal and structural design of the camera. The following paper discusses the effect of thermal gradients on the primary mirror optical performance. The discussion will also outline how the effects of temperature were used to design and implement a back focal length (BFL) control mechanism which will be used to modify optical performance on-orbit.

 0-8194-0855-7/92/$4.00

2. MARS OBSERVER CAMERA CONSTRUCTION

The MOC structure (narrow angle system), as shown in figure 1, is composed of four elements: The secondary mirror support assembly (SMSA), the main body structural assembly (MBSA), the aluminum base radiator, and the primary mirror. The unit is approximately 33.5 inches long. The SMSA and MBSA are composed of a Graphite/Epoxy (Gr/E) composite. The MBSA supports the primary mirror. The MBSA also supports the SMSA, which houses the secondary mirror and blocks stray light from the optics. The SMSA is only 0.020 inches thick but has a diameter of 15.45 inches and a surface area of over 1200 square inches. The structure was designed to be lightweight but stiff, allowing a stable and precisely metered optical device.

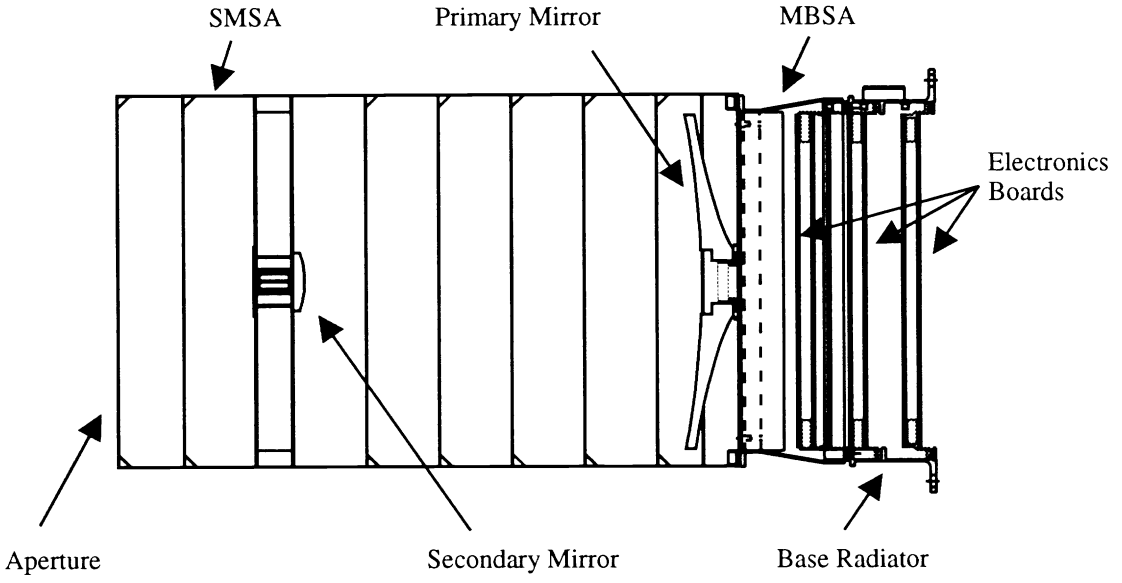

Figure 1, Mars Observer Camera (some parts removed for clarity)

2.1 Primary mirror

The primary mirror was designed to be rugged enough to survive the launch loads, yet it is supported by a low constraint mount so as not to cause the surface to deform at very low operational temperatures. Fused silica was chosen as the mirror substrate material because its CTE is a close match to that of the mirror's low-expansion Invar hub mount. The mirror is very lightweight (6.31 pounds) for its 13.84 inch diameter due to the unique single-arch construction. The mirror surface is coated with an enhanced silver coating which has low thermal emissivity ($\varepsilon<0.02$). The rear and remaining surfaces are polished for stress relief and are uncoated.

3. ANALYSIS

3.1 Thermal modelling

The MOC thermal behavior was analyzed using a 900-node finite difference model (FDM). The camera is dominated by radiative effects due to its relatively low thermal mass and large, exposed surface area. Thermal inputs to the model, therefore, consist largely of radiative sources such as the black-body and reflective albedo of Mars (0.15), the flux from the sun (442.2 BTU/hour•foot^2), and surrounding deep space. The relatively insignificant thermal mass of the SMSA allows large thermal gradients to be created depending on the orientation of the camera's surfaces to the external heat sources. The inputs are also time dependent, coinciding with the orbit of the spacecraft around Mars (period 118 minutes).

In contrast to the structure, the primary mirror has a much higher density (0.08 lb-mass/in^3) and heat capacity (80.5 cal/lb-mass•°C). Radiative exchange is still dominant, however, as the mirror is mounted to the camera structure through a relatively poor conduction joint. Therefore, the mirror experiences a time dependent thermal profile but with significantly smaller amplitudes and internal gradients than the camera structure.

The primary mirror portion of the FDM contains 50 nodes which are distributed about the optic axis in two-fold symmetry. Each quadrant contains 5 nodes evenly spaced radially, both on the top and bottom surface of the mirror. As the thickness of the mirror increases towards the mount, nodes are added internally. Conduction mainly occurs internally though some heat flows between the mirror and the mount. Radiative coupling of the top surface nodes to the external environment occurs through the camera aperture. Radiative coupling also exists between the surfaces of the mirror, the walls of the SMSA and the upper surface of the MBSA. The radiative coupling is highly complex in the region above the primary mirror due to the low emissivity of the mirror coating. Reflection produces convoluted ray paths which affect the overall coupling of the camera to the external environment. The ray-trace facility TRASYS was used to determine the ultimate view factors which result from this geometry.

The significant result of applying the FDM, for this discussion, was the discovery of a persistent (though time-varying) gradient profile through the body of the primary mirror. The gradient is largely radial (~0.4 °C/in), with some axial and circumferential components. Although the mirror is constructed of fused silica, a relatively low coefficient of thermal expansion (CTE) material, some concern was voiced over whether the gradient profile would produce unacceptable mirror surface figure displacements. Finite element modelling was used to address this concern.

3.2 Finite element modelling

Originally, the primary mirror finite element model (FEM) was constructed to verify structural integrity in the presence of vibratory and shock loading. This model consisted of over 900, 8-node solid elements distributed in a regular fashion about the optic axis. The number of elements per unit angle of azimuth was held fixed at all radial locations to cause an increase in linear element density near the mount, the location of highest stress. To be conservative, the boundary condition consisted of a rigid attachment to the vibration input datum to maximize its impedance. To adapt the model for use in a thermal strain investigation, 4-node quadrilateral plate elements were added to the upper surface to simulate the stiffness of the coating. The

boundary condition was allowed to be essentially free, being held fixed from motion in the axial direction on a single circumference at the mount.

The material properties of the glass and the coating are:

	Stiffness, PSI	CTE, /°C	Poisson Ratio
Fused Silica	1.06×10^{7}	3.069×10^{-7}	0.17
Enhanced Silver Coating	2.07×10^{7}	1.050×10^{-5}	0.31

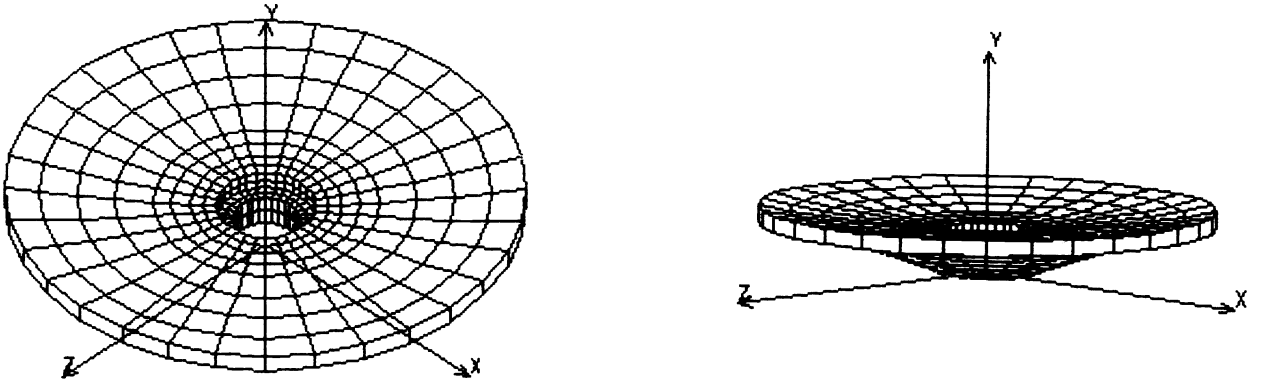

Figure 2, Primary mirror FEM

The temperature input for the FEM could not be taken directly from the FDM since no nodal position correlation existed between the models. Instead, a prescription of the temperature distribution was created by a 3-D, cylindrical coordinate polynomial regression of the FDM output. The temperature input was then generated by creating temperatures for each FEM node from the regression equation:

$$T = \sum_{i} A_i r^i + r \sum_{j} B_j \Theta^j + \sum_{k} C_k z^k + D$$

3.3 Finite element analysis

The decision to parameterize the temperature input led to an overall method of analyzing the behavior of the mirror. Due to the extremely small strains involved (order <10 ppm), application of of each component of the thermal prescription was posited to be linear and superposable. Each component of the gradient could be applied separately and the displacement effects added to create the combined displacement.

The separated temperature components are:
1. **Soak**-the equal offset in temperature of all nodes. This is the zeroth order regression parameter (D).
2. **Slope**-the radial (r) first order temperature gradient estimation which is the best fit of the first through nth order radial regression parameters.
3. **Axial**-the axial (z) first order temperature gradient estimation which is the best fit of the first through nth order axial regression parameters.
4. **Circumferential**-the circumferential (Θ) first order temperature gradient estimation which is the best fit of the first through nth order circumferential regression parameters.

Several FEM runs were made to find the displacements produced by individual temperature components. These results were then combined and compared to FEM runs where the complete temperature prescription was the input. The results were essentially identical.

The same reasoning was used to separate the CTE behavior of the glass from the effect of the coating/glass CTE mismatch. The separation was accomplished by making individual runs of the FEM model with either the glass or coating disabled. In the case of the coating, this was done by reducing the CTE of the bulk glass to zero and recording the effect of the coating strain alone. For the glass, the stiffness of the coating was reduced to zero producing the effect of an uncoated mirror. Combining both results yields the displacements of a coated mirror.

Next, verification runs were made which tested the validity of the FEM against data obtained about the behavior of the mirror in varied gravity vector orientations. The FEM was loaded with a 1g body force and compared to interferometry data of the camera upright and inverted. The test and FEM agreed to better than 95 percent. This test validated the model in terms of the stiffness of the glass and the coating and their behavior when coupled.

Following, a test run was completed which utilized a soak-only temperature distribution. When an object composed of homogeneous matter is subjected to an overall-intensive temperature shift, the new dimensions of the object are related to the original dimensions by a change of scale. The response of the primary mirror to a soak temperature, then, can be determined analytically using this scale-change analogy. Comparing the solution of a glass only scale change against a related soak-temperature FEM run showed excellent agreement.

With the verification complete, a suite of runs was made for the camera thermal environment which attempted to sample the entire parameter space of soak, slope, coating and glass. Some material properties were also varied to show the effect of gradient on other coating and glass types. This was done in an investigation of the viability of using ultra low expansion (ULE) glass for the primary mirror. In addition,

runs were made to investigate the effect of circumferential and axial gradients on the displacement of the mirror. The results of all FEM runs were then incorporated into an optical analysis of surface figure displacement which is discussed in the next section.

3.4 Correlation of the primary mirror surface displacement and optical characteristics.

The surface of the primary mirror can be described by the sag equation:

$$z = \frac{cx^2}{1 + \sqrt{1 - (k+1)c^2x^2}}$$

where c is the paraxial curvature of the surface (inverse of the radius of curvature (ROC)), k is the conic constant (nominally -1.010045 for this design) and z is the axial displacement (sag) from a plane tangent to the vertex, at the radial location, x, from the optic axis.

The necessary output from the primary mirror FEM, analyzed for each temperature profile, is the radial displacement (Δx) and axial displacement (Δz) of each mirror surface node from its nominal location. To find the new ROC, the Δx values are added to the nominal x values ($x+\Delta x$) and entered into the sag equation. Linear regression is then used to find the new c in the numerator by fitting the RHS to $z+\Delta z$. The c^2 term in the denominator is held constant during the regression, and then updated with the new value of c when the regression is completed. After the new value is inserted, the process repeats until the value of c converges. A constant term (z-offset) also results from the regression, which is due to a change in mirror thickness with soak temperature. The conic constant remains unaffected through this process.

When the best-fit ROC (1/c) is found, the maximum difference between the new sag equation and the axial displacements of the FEM nodes is, for any runs analyzed, typically between 3.6×10^{-7} and 3.6×10^{-8} inches ($\lambda/69$ to $\lambda/690$ at λ=0.6328 microns). The RMS error is typically 70% of the peak error. Therefore, the analysis demonstrates the temperature gradients analyzed produce essentially immeasurable wavefront error.

The ROC and thickness changes found through analysis only effect the BFL of the telescope. The relationship between ΔROC, thickness change (Δt), and ΔBFL is:

$$\Delta BFL = M^2(\tfrac{1}{2}\Delta ROC + \Delta t)$$

where M is the lateral magnification of the secondary mirror (approximately 7.5 for this design).

For the MOC primary mirror, the final result yields a ΔBFL per radial temperature gradient or slope of 0.0278 in/in•°C (measured from mirror hub to rim). For soak, the BFL changes 0.00062 in/°C for overall mirror temperature shift or soak. The axial and circumferential gradients produced surface figure movements of less than λ/20 and were ignored.

4. ACTIVE RADIUS OF CURVATURE (ROC) CONTROL

The result of the analysis of the mirror under a temperature gradient led the design team to investigate the possibility of applying this effect intentionally to control the BFL of the camera. As originally stated, the sensitivity of the camera's BFL to changes in optical path lengths is extremely high. Attempts at athermalizing the SMSA were met with limited success. Analysis indicated thermal displacements were likely to cause unacceptable excursions (order 0.02 inches) in BFL over the Martian year. In the original conception, active BFL control was proposed but rejected for reliability reasons. Thermal control represented an opportunity to modify camera BFL in-flight with a simple system of heaters and power controllers. No moving parts or other low reliability systems were needed.

The basic design of the ROC controller is two Tayco strip heaters, one which is circumferentially mounted to the SMSA surrounding the primary mirror (rim heater) and another mounted to a conical aluminum support attached to the primary mirror mount structure (hub heater). Heat transfer occurs by radiative coupling between the heaters and the mirror. The view factors which control the effectiveness of the radiative coupling are relatively high due to the proximity of the heaters to the mirror and the high emissivity of both.

Placing heaters at both the edge and the hub of the mirror allow bi-polar control of the mirror's ROC about the unperturbed position. The rim heater creates a radial slope gradient across the mirror which is opposite in sign to the radial slope gradient produced by the hub heater.

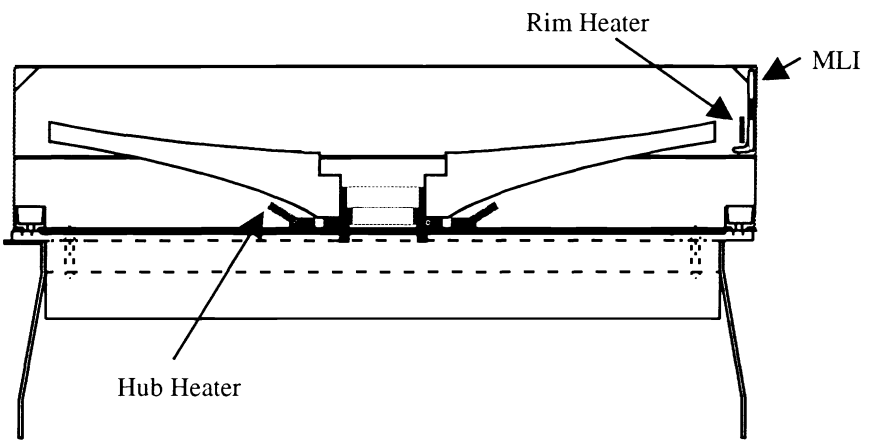

Figure 3, ROC controller heater placement

The placement of the heaters are as shown in figure 3. Both heaters have etched foil designs which contain a fully independent set of traces for redundancy. The edge heater is sewn to an MLI blanket which insulates it from the SMSA MLI blankets, minimizing heat loss. The hub heater is bonded to the underside of a thin, conical aluminum section which is mounted to the MBSA through three low conduction G10 spacers. The aluminum piece is warmed by the heater which then radiates to the mirror through a high emissivity black anodize coating. The heater, which faces the MBSA, is coated with a very low emissivity radiation isolation tape (Sheldahl type G401000).

The heaters are powered by independent, fully redundant Solid State Relays (SSR). These devices allow the instrument's microprocessor to switch the spacecraft's 28 volt bus across the heaters in an adjustable duty cycle, thus adjusting either heater power to any level desired. The cycling period is short compared to the thermal reaction time of the primary mirror, which is on the order of hours. As the MOC electronics are fully redundant, the two redundant traces in each heater are controlled by separate sets of electronics.

The thermal behavior of the heaters and the response of the primary mirror was included in the FDM of the MOC. Several power input values were modelled. The results indicated acceptable actuation authority with the power available. However, use of either heater tended to increase the soak temperature of the mirror, and hence change the BFL of the camera. This reduces the effectiveness of the rim heater while increasing the effectiveness of the hub heater. Fortunately, the rim heater is better able to create its thermal gradient than the hub heater, thereby reducing the asymmetry between them.

5. TEST

Verification of the installed first generation ROC controller was accomplished at a thermal-vacuum chamber at TRW in Redondo Beach, California in August of 1991. The purpose of this test was to verify the behavior of the camera structure when subjected to a variety of thermal inputs. The first generation ROC controller was only equipped with the "rim" heater operational due to schedule constraints. The heater was also powered externally, as no electronics were integrated into the camera for this test.

The test set-up was composed of the chamber, the MOC and various pieces of fixturing and instrumentation as shown in figure 4. The chamber was a large, cubic structure with thermally controlled walls which could be heated to 150° F or cooled to liquid nitrogen temperatures. The MOC was mounted in the chamber on a vibration isolation table and oriented horizontally so the aperture would be accessible through a window in one wall. To control temperatures, the camera and isolation table were covered with strip heaters, MLI, and fully instrumented with thermocouples. Thermocouples were also placed on the primary mirror itself.

Various temperature control schedules were created which would cause the heaters to warm the camera to predicted on-orbit temperatures. Cooling occurred to the cold walls which acted as continuous heat sinks. The mirror was primarily controlled, for purposes of on-orbit conditioning, by a heated plate suspended in front of the aperture. This plate, which could be raised or lowered from outside the chamber, broadly emulated a predicted average Martian thermal effect.

To measure the ΔBFL of the MOC while in the chamber, a laser interferometer was employed which measured the location of best focus in relation to a reference reticle. Figure 5 outlines the focus measurement

set-up. A benefit of using this test measurement method is the ability to detect mirror surface irregularity in addition to measuring focus.

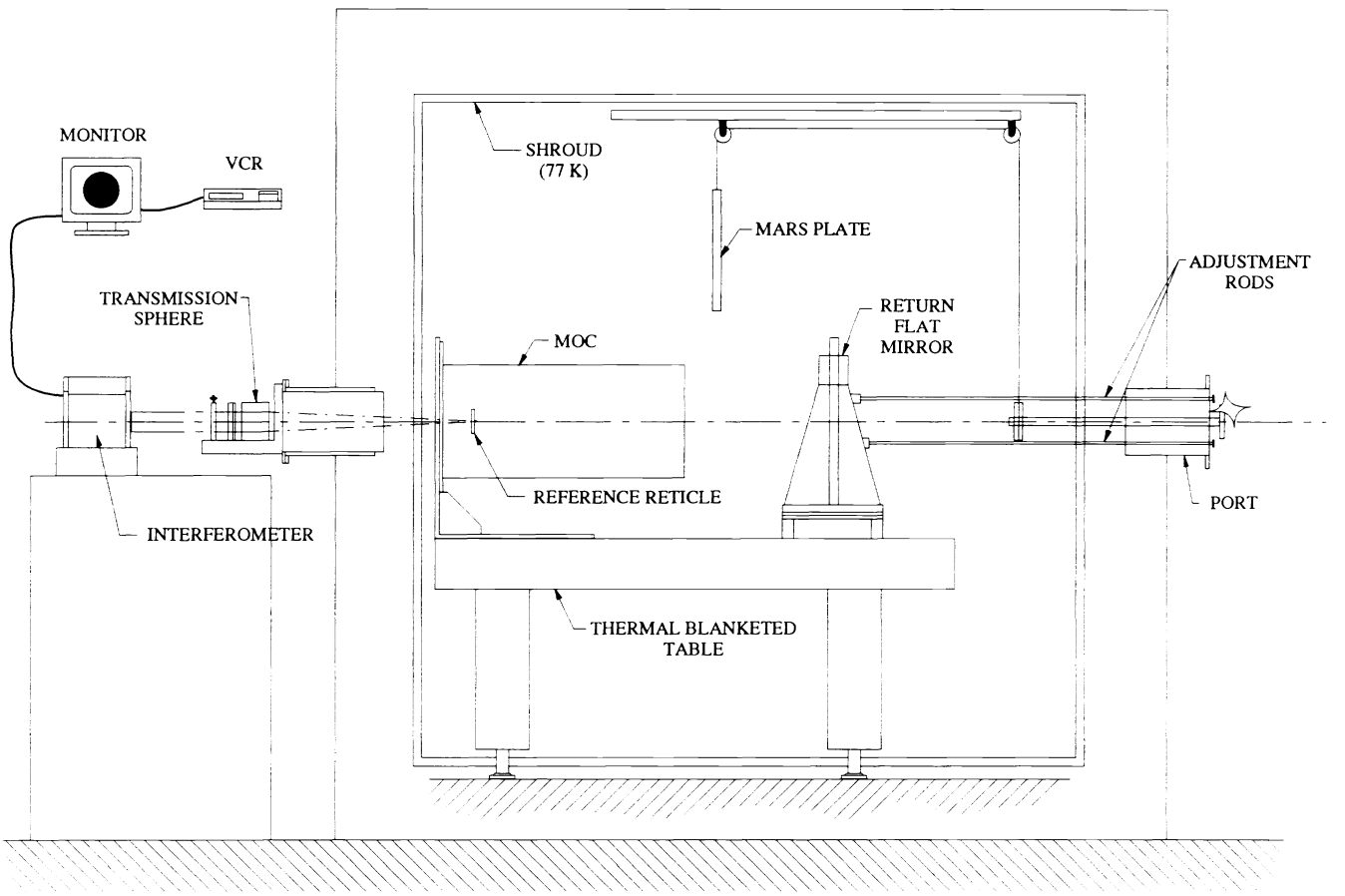

Figure 4, MOC thermal-vacuum chamber test set-up

The testing itself revolved around two thermal cases from the on-orbit thermal modelling results. These were for Mars in the aphelion and perihelion orbital positions. In either case, the primary mirror exhibits some radial thermal gradient naturally without heaters.

For the perihelion cases, the test of the ROC controller was made at 2 watts and at 4 watts. The results of these tests showed a change in the BFL of the camera of 0.0137 inches and 0.0363 inches, respectively. For the aphelion case, only a 2 watt case was attempted, with a resulting shift of 0.0044 inches. In both cases, the sign of the focal length motion was consistent with the model.

The results from thermal-vacuum testing indicated the first generation ROC controller worked but at only half of the effectiveness predicted. This was confirmed through the monitoring of the primary mirror

temperature during the test which indicated a developed slope gradient far less than hoped. However, the actuation range was still demonstrated to be several times the camera's depth of focus. In addition, for the range of temperature cases, no mirror surface irregularity was found, substantiating the earlier regression analysis. Following the test, the rim heater was redesigned increasing its radiative coupling to the mirror and minimizing the parasitic heat loss to the SMSA. The hub heater was also assembled into the unit.

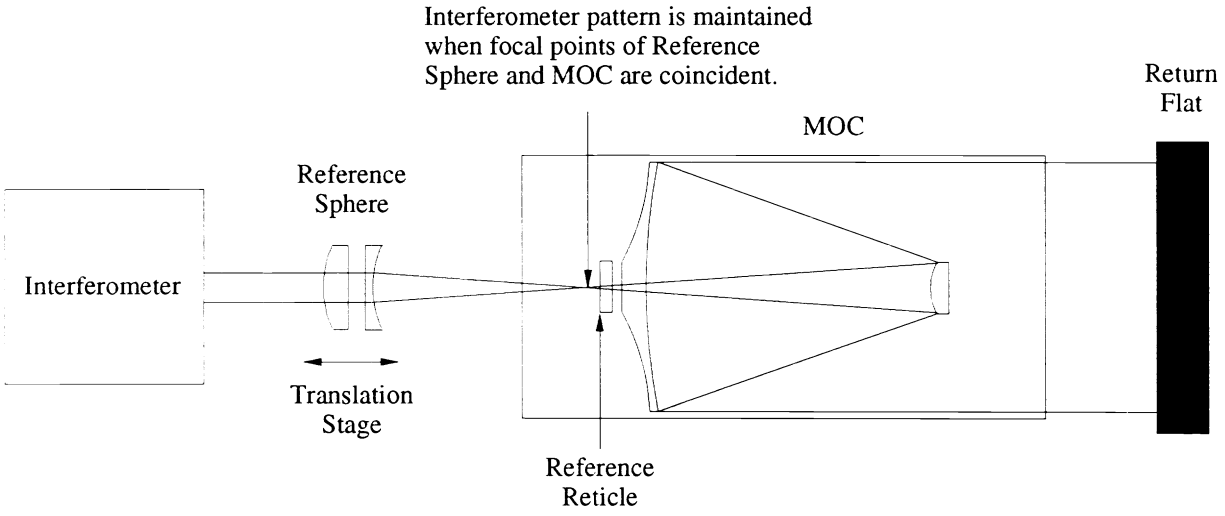

Figure 5, MOC interferometric test set-up. MOC axial focal point displacements can be measured directly by the reference sphere displacement required to regain the interferometric pattern.

In January of 1992, another thermal-vacuum test was conducted at TRW where the ROC controller was again tested. Here, the complete ROC controller system was exercised including electronics. In this case, however, the camera was fully assembled making interferometric measurement impossible. Instead, a modulation transfer function (MTF) bar target was imaged by the complete MOC system. Analysis of the images showed a ΔBFL of approximately 0.05 inches for the rim heater at 4 watts and 0.02 inches for the hub heater also at 4 watts.

This test confirmed the operation of the flight version of the ROC controller. While the actuation was still not as large as expected, it is completely adequate for the expected on-orbit needs.

6. CONCLUSIONS

The Mars Observer Camera optical performance was shown to be substantially effected by primary mirror temperature gradients. BFL was significantly altered with negligible surface figure aberrations. This effect was successfully used to control the BFL of the camera in a high reliability system. This system will be used to adjust camera BFL while on orbit at Mars. The significant findings from this work are:

1) Mild temperature gradients can have a large effect on mirror surface figure, even for relatively low CTE materials.

2) In the case of the MOC primary mirror, radial slope gradients produced purely ROC shifts, with little additional aberration.

3) A high reliability solid-state ROC controller using the thermal gradient effect was implemented and verified by test.

7. ACKNOWLEDGEMENTS

The investigation of the effects of thermal gradients on the MOC primary mirror and the implementation of ROC control was undertaken by several members of the MOC design team. They are: Roger Bartlett of Foster Engineering for FDM analysis, Larry Steimle of JPL for thermal-vacuum and interferometric testing, Gary Pollitt of GP Engineering for the ROC controller electronic design and Mike Ravine of Altadena Instruments and Hugh Von Delden of JPL for the ROC controller heater design. The authors also wish to thank Ed Danielson, the MOC Instrument Manager and Dr. Michael Malin, MOC Principal Investigator for their support of this effort. In preparation of this manuscript, Elaine Lindelef of Altadena Instruments provided invaluable assistance in creating graphics and publishing the final document. This work was funded by the Mars Observer JPL Contract No. 957575.

8. REFERENCES

1. M. C. Malin, G. E. Danielson, M. A. Ravine, and T. A. Soulanille, "Design and development of the Mars Observer Camera," *Int. J. Imag. Syst. Tech.*, Vol. 3, pp. 76-91, 1991.
2. A. R. Telkamp, and E. A. Derby, "Design considerations for composite materials used in the Mars Observer Camera," SPIE Vol. 1303, Advances in Optical Structure Systems, pp. 416-436, Orlando, April 1990.
3. A. R. Telkamp, "Recent developments with the Mars Observer Camera," SPIE conference 1690, Design of Optical Instruments, Orlando, April 1992.